*NIST Technical Note 1530*

# UNCERTAINTY ANALYSIS FOR NIST NOISE-PARAMETER MEASUREMENTS

**James Randa**

*NIST Technical Note 1530*

# UNCERTAINTY ANALYSIS FOR NIST NOISE-PARAMETER MEASUREMENTS

James Randa

*Electromagnetics Division*
*Electronics and Electical Engineering Laboratory*
*National Institute of Standards and Technology*
*325 Broadway*
*Boulder, CO 80305*

March 2008


**U.S. Department of Commerce**
*Carlos M. Gutierrez, Secretary*

**National Institute of Standards and Technology**
*James M. Turner, Acting Director*

Certain commercial entities, equipment, or materials may be identified in this document in order to describe an experimental procedure or concept adequately. Such identification is not intended to imply recommendation or endorsement by the National Institute of Standards and Technology, nor is it intended to imply that the entities, materials, or equipment are necessarily the best available for the purpose.

---

National Institute of Standards and Technology
Technical Note 1530
Natl. Inst. Stand. Technol.
Tech. Note 1530
34 pages (March 2008)
CODEN: NTNOEF

U.S. Government Printing Office
Washington: 2008

For Sale by the
Superintendent of Documents
U.S. Government Printing Office
Stop SSOP,
Washington, DC 20402-0001
Phone: (202) 512-1800
Fax: (202) 512-2250
Internet: bookstore.gpo.gov

**CONTENTS**

# UNCERTAINTY ANALYSIS FOR NIST NOISE-PARAMETER MEASUREMENTS

James Randa

Electromagnetics Division
National Institute of Standards and Technology
Boulder, CO 80305

The uncertainty analysis is presented for NIST measurements of noise parameters of amplifiers and transistors, in both connectorized (coaxial) and on-wafer environments. We treat both the *X*-parameters, which are based on the wave representation of the noise correlation matrix, and the traditional IEEE noise parameters. An overview of the Monte Carlo program used to evaluate the type-B uncertainties is included.

*Keywords: amplifier noise, measurement uncertainty, Monte Carlo, noise measurement, noise figure, noise parameters, transistor noise, uncertainty*

## 1. INTRODUCTION

Some time ago, what is now the Electromagnetics Division of the National Institute of Standards and Technology (NIST) developed the capability to measure noise parameters of amplifiers [1,2]. Recently, modified methods and analysis have been developed and have been applied both to amplifiers [3] and to transistors [4], the latter in an on-wafer environment. For such measurements to be meaningful, the results must be accompanied by corresponding uncertainties. Many complications arise in the analysis for these measurements, and it is the purpose of this paper to document and perhaps clarify the procedures used to estimate the standard uncertainties [5] in the measured noise parameters.

The contributions to the standard uncertainty are divided into two groups. Generally, type-A uncertainties are those that are determined by statistical means, and type-B are all others. The standard or combined uncertainty ($u_c$) in a quantity is the root sum of squares (RSS) of the type-A and type-B uncertainties,

$$u_c = \sqrt{u_A^2 + u_B^2}\ . \tag{1}$$

Noise parameters are computed by performing a least-squares fit to an over-determined system of equations obtained by measuring the output noise temperature (or power) for each of a number of different input terminations connected to the amplifier or transistor under test. The type-A uncertainties can be computed from the covariance matrix of the fitted parameters, but the type-B uncertainties require more effort. The uncertainties in the underlying or input quantities, such as reflection coefficients, measured noise temperatures, etc., are known or can be estimated; but the problem of propagating these underlying uncertainties to compute

uncertainties in the output noise parameters does not admit a simple analytical solution. Therefore, a Monte Carlo approach is used for the type-B uncertainties. Matters are further complicated by the fact that it is convenient to perform our analysis in terms of one set of noise parameters (what we call the *X* parameters), but we need to express our results and uncertainties in terms of a different set (the IEEE noise parameters) that is in near-universal use.

In the next section we present the theoretical framework used in the analysis. Section 3 reviews the measurement methods, both on-wafer and off-wafer. The uncertainty analysis for the off-wafer, connectorized case is presented in Section 4, followed by the on-wafer case in Section 5. Section 6 contains a summary. There are two appendices: Appendix A presents the Jacobian matrix for the transformation from our *X* parameters to the IEEE noise parameters, and Appendix B gives an overview of the Fortran program used to evaluate the type-B uncertainties.

## 2. THEORETICAL FRAMEWORK

### 2.1 Noise Parameters in the Wave Representation

Our general theoretical framework was set out in Reference [6]. It follows the wave representation formulated by Wedge and Rutledge [7]. For a linear two-port, such as an amplifier or transistor, the amplitudes of the incident and outgoing waves are related by

$$\boldsymbol{b} = \boldsymbol{S}\boldsymbol{a} + \boldsymbol{c}\,, \tag{2}$$

where $\boldsymbol{a}$ and $\boldsymbol{b}$ are two-dimensional vectors whose elements are the incident and outgoing wave amplitudes, as indicated in Fig. 1, $\boldsymbol{S}$ is the usual 2×2 scattering matrix, and $\boldsymbol{c}$ is a two-dimensional vector whose elements are amplitudes of the waves emerging from the two ports even in the absence of any input waves, due to the intrinsic noise of the device. Although this paper deals with noise parameters of both transistors and amplifiers, the figures will be drawn with only the amplifier symbol, or with a generic box, and we will use DUT (device under test) to refer to either an amplifier or a transistor. We use a normalization in which the wave amplitudes squared have dimensions of spectral power density, power per frequency interval. When we refer to noise temperature, we take it to mean the available noise spectral power density divided by Boltzmann's constant $k_B$.

The noise properties of the two-port are characterized by the (intrinsic) noise correlation matrix $\boldsymbol{N}$, defined by

$$N_{ij} \equiv \left\langle c_i c_j^* \right\rangle, \tag{3}$$

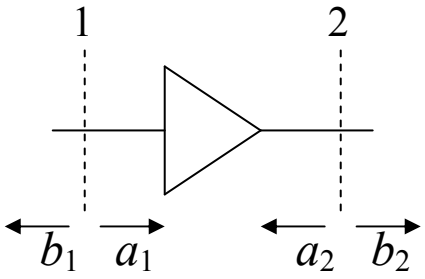


Figure 1. Reference planes for amplifier noise parameters.

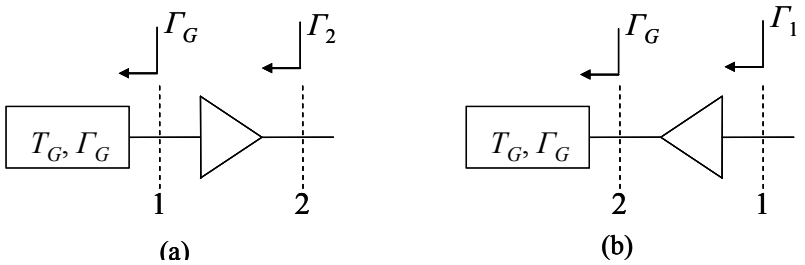


Figure 2. Forward (a) and reverse (b) measurement configurations.

where the brackets indicate time or ensemble average (assumed to be equal). We find it convenient to work with temperature variables corresponding to scaled elements of the noise correlation matrix. We define

$$k_B X_1 \equiv \left\langle |c_1|^2 \right\rangle, \; k_B X_2 \equiv \left\langle |c_2 / S_{21}|^2 \right\rangle, \; k_B X_{12} \equiv \left\langle c_1 (c_2 / S_{21})^* \right\rangle. \tag{4}$$

Dividing each $c_2$ by $S_{21}$ effectively refers all four noise parameters ($X_1$, $X_2$, $ReX_{12}$, $ImX_{12}$) to the input plane 1. In fact, it can (and will) be seen that $X_2$ is equal to the effective input noise temperature for a reflectionless input termination, $X_2 = T_{e,0}$ , sometimes also called the "50 Ω noise temperature." $X_1$ is the intrinsic noise emerging from the input port (1); it is closely related to the $T_{rev}$ of Wait and Engen [1],

$$T_{rev} = \frac{X_1}{\left(1 - |S_{11}|^2\right)}. \tag{5}$$

Two different measurement configurations are used in the NIST noise-parameter measurements: the "forward" configuration of Fig. 2(a) and the "reverse" configuration of Fig. 2(b). The forward configuration is the one usually used for noise-parameter measurements, but the reverse configuration can also be used, and it provides a very good determination of the parameter $X_1$. The reverse configuration is particularly useful in the on-wafer case for poorly matched transistors [8]. The output noise temperature for the two configurations can be written in terms of the scattering and noise parameters of the amplifier and the reflection coefficient $\Gamma_G$ and noise temperature $T_G$ of the source or generator. For the forward configuration, the equation is

$$T_2 = \frac{|S_{21}|^2}{\left(1-|\Gamma_2|^2\right)}\left\{\frac{\left(1-|\Gamma_G|^2\right)}{|1-\Gamma_G S_{11}|^2}T_G + \left|\frac{\Gamma_G}{1-\Gamma_G S_{11}}\right|^2 X_1 + X_2 + 2\,\mathrm{Re}\left[\frac{\Gamma_G X_{12}}{1-\Gamma_G S_{11}}\right]\right\}, \quad (6)$$

and for the reverse configuration it takes the form

$$T_1 = \frac{1}{\left(1-|\Gamma_1|^2\right)}\left\{\frac{|S_{12}|^2\left(1-|\Gamma_G|^2\right)}{|1-\Gamma_G S_{22}|^2}T_G + \left|\frac{S_{12}S_{21}\Gamma_G}{1-\Gamma_G S_{22}}\right|^2 X_2 + X_1 + 2\,\mathrm{Re}\left[\frac{S_{12}S_{21}\Gamma_G X_{12}^*}{1-\Gamma_G S_{22}}\right]\right\}, \quad (7)$$

where $\Gamma_2$ is the reflection coefficient of the generator-amplifier combination at plane 2 in Fig. 2(a), and $\Gamma_1$ is the reflection coefficient of the generator-amplifier combination at plane 1 in Fig. 2(b). In performing the fits, the parameters to be determined are the $X$'s and the "reduced gain," defined by $G_0 \equiv |S_{21}|^2$. All other S-parameters, including the phase of $S_{21}$, are taken from measurements on a commercial vector network analyzer (VNA).

### 2.2 Relation to IEEE Noise Parameters

Although many different sets of noise parameters have been suggested, the set in most widespread use is the IEEE set [9]. It is therefore desirable to present any measurement results in terms of the IEEE set, in addition to the results for the $X$'s. Even within the IEEE set, there are several variants; we use the one in which the effective input noise temperature $T_e$ is given by

$$T_e = T_{\min} + t\frac{\left|\Gamma_{opt} - \Gamma_G\right|^2}{\left|1+\Gamma_{opt}\right|^2\left(1-|\Gamma_G|^2\right)}, \quad (8)$$

where $\Gamma_G$ is the reflection coefficient of the input termination at plane 1, and the four noise parameters are $T_{min}$, $t$, and the complex $\Gamma_{opt}$. The parameter $t$ is related to the noise resistance $R_n$ by $t = 4R_nT_0/Z_0$, where $T_0 = 290$ K and $Z_0$ is the reference impedance, commonly taken to be 50 Ω.

To make the connection between the $X$-parameters and the IEEE noise parameters, we force eq. (6) into the form

$$T_2 = G_{av}\left(T_e + T_G\right), \quad (9)$$

where $G_{av}$ is the available gain,

$$G_{av} = \frac{|S_{21}|^2}{\left(1-|\Gamma_{GS}|^2\right)}\frac{\left(1-|\Gamma_G|^2\right)}{|1-\Gamma_G S_{11}|^2}. \quad (10)$$

This yields the expression for $T_e$ in terms of the $X$-parameters,

$$T_e = \frac{|\Gamma_G|^2}{\left(1-|\Gamma_G|^2\right)} X_1 + \frac{|1-\Gamma_G S_{11}|^2}{\left(1-|\Gamma_G|^2\right)} X_2 + \frac{2}{\left(1-|\Gamma_G|^2\right)} \mathrm{Re}\left[\Gamma_G \left(1-\Gamma_G S_{11}\right)^* X_{12}\right], \qquad (11)$$

which can be compared with eq. (8) to derive the relationship between the *X*-parameters and the IEEE noise parameters. Happily, Wedge and Rutledge [7] have done the bulk of the algebra for us, obtaining the relationship between the noise correlation matrix of eq. (3) and the IEEE noise parameters. We then need only use the definitions of eq. (4) to obtain

$$\begin{aligned} X_1 &= T_{\min}\left(|S_{11}|^2 - 1\right) + \frac{t|1-S_{11}\Gamma_{opt}|^2}{|1+\Gamma_{opt}|^2}, \\ X_2 &= T_{\min} + \frac{t|\Gamma_{opt}|^2}{|1+\Gamma_{opt}|^2}, \\ X_{12} &= S_{11}T_{\min} - \frac{t\Gamma_{opt}^*\left(1-S_{11}\Gamma_{opt}\right)}{|1+\Gamma_{opt}|^2}. \end{aligned} \qquad (12)$$

The inverse relations are

$$\begin{aligned} t &= X_1 + |1+S_{11}|^2 X_2 - 2\,\mathrm{Re}\left[(1+S_{11})^* X_{12}\right], \\ \Gamma_{opt} &= \frac{\eta}{2}\left(1 - \sqrt{1-\frac{4}{|\eta|^2}}\right), \\ T_{\min} &= \frac{X_2 - |\Gamma_{opt}|^2\left[X_1 + |S_{11}|^2 X_2 - 2\,\mathrm{Re}\left(S_{11}^* X_{12}\right)\right]}{\left(1+|\Gamma_{opt}|^2\right)}, \end{aligned} \qquad (13)$$

where

$$\eta = \frac{X_2\left(1+|S_{11}|^2\right) + X_1 - 2\,\mathrm{Re}\left(S_{11}^* X_{12}\right)}{\left(X_2 S_{11} - X_{12}\right)}. \qquad (14)$$

Thus, if the S-parameters are known, the IEEE parameters can be calculated from the *X*-parameters, and vice versa. Additional work is required to transform the uncertainties in the noise parameters. That point is addressed below, in Section 4.

### 2.3 Physical Bounds

Basic physics and mathematics place certain constraints on the noise parameters. Some of the constraints are obvious in either the IEEE representation or the $X$ representation. For example, $T_{min}$, $t$, $X_1$, and $X_2$ must all be positive, and $2|X_{12}| \le X_1 + X_2$. Some are less obvious, such as $|\eta| \ge 2$. This last inequality can be proved by using eq. (4) to write the numerator and denominator of eq. (14) in terms of the $c$ wave amplitudes. The numerator can be put in the form

$$X_2\left(1+|S_{11}|^2\right)+X_1-2\,\mathrm{Re}\left(S_{11}^* X_{12}\right)=\left\langle\left|\left(\frac{c_2}{S_{21}}\right)^*\right|^2+\left|\frac{c_2 S_{11}}{S_{21}}-c_1\right|^2\right\rangle, \tag{15}$$

whereas the denominator is given by

$$X_2 S_{11}-X_{12}=\left(\frac{c_2}{S_{21}}\right)^*\left(\frac{c_2 S_{11}}{S_{21}}-c_1\right). \tag{16}$$

That $|\eta| \ge 2$ then follows from the Schwarz inequality.

In actual measurements, as well as in the simulations in the Monte Carlo program discussed below, it is possible to obtain unphysical results that violate these bounds. This is rare when measuring well-matched amplifiers, but it is not uncommon when measuring poorly matched, very low-noise transistors on a wafer. Small measurement errors can conspire to yield fitted results for the noise parameters that are slightly (or even dramatically) outside the physical bound rather than slightly within it. One approach to this problem would be to constrain the fitting procedure so that the fitting parameters range only over physically allowed values. Instead, we choose to perform an unconstrained fit and to test whether the result satisfies the physical bounds. This has the advantage of alerting us when the measurement results prefer an unphysical solution for the noise parameters, rather than just finding the best physical solution. (It is also considerably easier than imposing this set of constraints in the fit.) We will return to this point when we discuss the Monte Carlo program below.

## 3. MEASUREMENT METHOD

Basically, the measurement method for either off-wafer ("connectorized") amplifiers or on-wafer transistors (or amplifiers) consists of connecting a series of different, known terminations to one of the ports of the device under test and measuring the resulting noise temperature at the other port. The noise parameters are then computed by performing a weighted least-squares fit using eqs. (6) and (7). Most or all of the measurements are performed in the forward configuration of Fig. 2(a), in which the known termination ($\Gamma_{G,i}$, $T_{G,i}$) is connected to the input port, and the noise temperature ($T_{2,i}$) is measured at the output port. In the case of poorly matched devices, typically transistors on a wafer, it is advantageous to also perform at least one reverse measurement, as in Fig. 2(b). The termination used for the reverse measurement is typically an ambient-temperature matched load. In principle, more than one reverse measurement

could be used; we are currently investigating the efficacy of that. For well-matched amplifiers, the reverse measurement does not improve the noise-parameter uncertainties [6], and so we do not use it in the fit for the noise parameters. In such cases, we often perform a reverse measurement and use it as a check, comparing the measured value for $T_1$ to the value predicted by eq. (7) with the values of the noise parameters that have been measured.

The set of input terminations typically comprises about eight ambient-temperature terminations and one well-matched non-ambient noise source (usually hot). The input states are discrete reflective or matched loads, connected manually to the appropriate port; we do not use a tuner. We are currently developing an automated unit to switch automatically among the different input terminations [10]. The ambient-temperature terminations include one matched load and several reflective terminations chosen to provide adequate coverage of the complex-$\Gamma$ unit circle. Although we have not made a great effort to optimize the choice of input reflection coefficients, simulations have shown that we would gain little by using an optimized set, such as is used by some commercial systems. The reflection coefficients of the input terminations and the S-parameters of the device under test are measured on a VNA. As noted above, the quantity $G_0 \equiv |S_{21}|^2$ is treated as a free parameter in the fit; the fitted value usually agrees very well with the value obtained from the VNA measurements. Since the same set of terminations is used across the entire range of measurement frequencies, the reflection coefficients of the individual terminations shift with frequency. The patterns of the reflection coefficients in the complex plane at three representative frequencies in the 8 GHz to 12 GHz band are shown in Fig. 3.

The noise temperatures of the ambient input terminations are taken to be the noise temperature corresponding to 296.15 K,

$$T_{G,i} = \frac{hf}{\left(e^{hf/(k_B \cdot 296.15K)} - 1\right)}, \tag{17}$$

where $T_{G,i}$ is the noise temperature of termination $i$, assumed to be one of the ambient-temperature terminations. The noise temperature of the non-ambient input termination is measured on the NIST coaxial radiometer NFRad [11], as are all output noise temperatures.

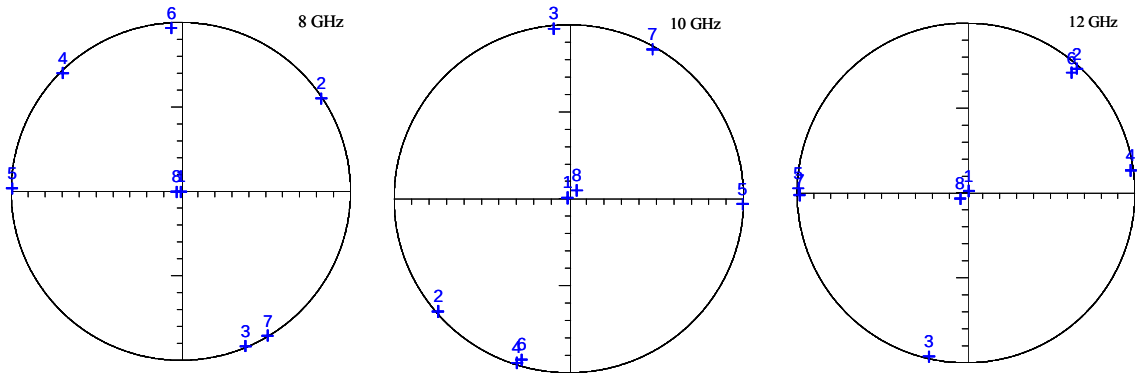


Figure 3. Reflection coefficients of input terminations relative to the unit circle at three frequencies.

Measurement of the output noise temperature for each input termination $i$ yields a set of measured values for $T_2$, which we call $T_{2,i}$(meas), and possibly one or more measured values for the reverse configuration, $T_1$, which we call $T_{1,i}$(meas). Each measured value is accompanied by a standard uncertainty, $u(T_{2,i})$ or $u(T_{1,i})$. For each measurement, we also have a corresponding expression for the output noise temperature from eq. (6) or (7). The reflection coefficients and S-parameters in these expressions have been measured, and so the only remaining unknowns are the noise parameters. We refer to the expressions as $T_{2,i}(X)$ and $T_{1,i}(X)$, where the $X$ is understood to include $G_0$, as well as $X$'s. From measurements of the forward configuration, we obtain a set of equations of the form

$$T_{2,i}(meas) = T_{2,i}(X), \tag{18}$$

for $i = 1,\ldots,N_{fwd}$, where $N_{fwd}$ is the number of forward measurements. If we include a measurement in the reverse configuration, we obtain an additional equation of the form

$$T_{1,i}(meas) = T_{1,i}(X). \tag{19}$$

These equations can be used to determine the noise parameters and $G_0$. To do so, we perform a weighted, least-squares fit, minimizing the function

$$\chi^2 = \sum_{i,fwd} \left( \frac{T_{2,i}(meas) - T_{2,i}(X)}{u(T_{2,i})} \right)^2 + \sum_{i,rev} \left( \frac{T_{1,i}(meas) - T_{1,i}(X)}{u(T_{1,i})} \right)^2, \tag{20}$$

where the first sum runs over the forward measurements, and the second sum over the reverse measurements. For well-matched, packaged amplifiers, we do not typically use the reverse measurements in the determination of the noise parameters, and consequently the second sum is absent. In that case, the equations are all of the form of eq. (6), which can easily be put into linear form by defining the variables $Z_1 = G_0X_1$, $Z_2 = G_0X_2$, $Z_{12} = G_0X_{12}$, $Z_5 = G_0$. In terms of the $Z$'s, the set of equations becomes linear. A commercial fitting program is used to minimize $\chi^2$. If only forward measurements are used, a linear fitting program would suffice, but if reverse measurements are present, the problem cannot be reduced to a set of linear equations. In practice, we use the nonlinear fitting program in all cases, because it is the only one that provides the full covariance matrix, which we need in order to compute the uncertainties in the IEEE noise parameters. The linear fitting program is used on the (sub)set of forward measurements to obtain an initial guess for input to the nonlinear fitting program. The nonlinear fitting program uses a modified Levenberg-Marquardt method (see, e.g., [12]) to solve a nonlinear regression model using least squares.

## 4. UNCERTAINTIES I: OFF-WAFER, COAXIAL REFERENCE PLANES

### 4.1 Type-A Uncertainties

Type-A uncertainties are those that are evaluated by a statistical analysis of a series of observations [5]. In our case, where the parameters are determined by a fit to an over-determined

system of equations, the packaged fitting program returns the covariance matrix $V_{ij}$ for the fitting parameters, and the type-A uncertainties are given by the square roots of the diagonal elements,

$$u_A(X_i) = \sqrt{V_{ii}(X)}\ , \tag{21}$$

where $X_i$ represents any of the five fitting parameters ($X$'s and $G_0$).

Since the parameters in most common use are the IEEE parameters, we also need to evaluate the uncertainties in them. Because the fit is performed in terms of the $X$-parameters, the fitting program does not return values or a covariance matrix for the IEEE parameters. The IEEE parameter values are computed from the $X$-parameters by use of eqs. (13) and (14), and the covariance matrix for the IEEE parameters must be computed from the $X$-parameter covariance matrix by use of the Jacobian matrix for the transformation. If we use $I_i$ to represent one of the five IEEE parameters (including $G_0$), then the type-A uncertainties in the IEEE parameters are given by

$$\begin{aligned} u_A(I_i) &= \sqrt{V_{ii}(IEEE)}\ , \\ V_{ij}(IEEE) &= \sum_{i',j'=1}^{5} \frac{\partial I_i}{\partial X_{i'}} \frac{\partial I_j}{\partial X_{j'}} V_{i'j'}(X)\ . \end{aligned} \tag{22}$$

Calculation of the elements of the Jacobian matrix ($\partial I_i/\partial X_{i'}$) is straightforward but tedious, and the results are lengthy and unenlightening. They are relegated to Appendix A.

### 4.2 Type-B Uncertainties

Type-B uncertainties are those that are evaluated by any means other than the statistical analysis of a series of observations. In our noise-parameter measurements, these uncertainties arise due to possible errors in the input parameters, which include the amplifier S-parameters, all measured reflection coefficients, the temperature of the ambient-temperature terminations, the noise temperature of the non-ambient termination(s), and the measured output noise temperatures. We know or can estimate all these input uncertainties, but the problem of how they propagate into uncertainties in the noise-parameters does not admit a simple analytical solution. We therefore adopt a Monte Carlo approach, a good description of which can be found in Reference [13]. Our Monte Carlo procedure has been described previously in References [6] and [14]. Here we present a somewhat more detailed and updated account.

The Monte Carlo uncertainty evaluation is built around the generation of simulated results for the measurements that were actually performed. These simulated measurement results are analyzed in the same way as are the real data, yielding simulated values for the noise parameters. This process is repeated a large number of times, and the distribution of values obtained for each noise parameter is used to compute its uncertainty. One full simulation of all the measurements that were actually performed will be referred to as a "set" of measurements, and the number of simulated measurement sets will be denoted $N_{sim}$. We choose $N_{sim}$ to be large enough that the computed uncertainties are approximately independent of $N_{set}$. A value of $N_{sim} = 10{,}000$ is usually more than sufficient, but for poorly matched transistors, it is occasionally necessary to use larger values. In all cases, we use a large enough value that any

further increase in $N_{sim}$ changes the uncertainties by at most 10 % of their values. In most cases, the uncertainties are within a few percent of their asymptotic values.

Each simulated measurement is performed by choosing a number randomly from the probability distribution for that physical quantity. The distribution is constrained to have an average value equal to the true value and a standard deviation equal to the standard uncertainty for that quantity. We use the real measurement results as the true values. Normal distributions are assumed for all quantities except for the ambient temperature, for which a rectangular distribution is used, to better model the effect of a thermostatically controlled laboratory temperature. (The program also allows the user to choose a normal distribution for the ambient temperature, but we do not usually use this. It makes virtually no difference in practice.) For each measurement set, we first simulate measurement of the input parameters; these include the amplifier S-parameters, the reflection coefficients of all input terminations, the noise temperatures of all terminations, and the output reflection coefficients, $\Gamma_{2,i}$ in Fig. (2), if they are measured. (There is an option of measuring $\Gamma_{2,i}$ directly or of computing it by cascading $\Gamma_{G,i}$ with the S-parameters.) To simulate the measurement of the output noise temperatures, we must first compute the true values from eq. (6) (for the forward configuration) or eq. (7) (for the reverse configuration), using the true values for all quantities on the right hand side.

To simulate a measurement (of a quantity $y$, for example) we merely add a random error term $\delta y$ to the true value $y_0$,

$$y(sim) = y_0 + \delta y, \tag{23}$$

where $\delta y$ is chosen randomly from the appropriate distribution (normal or rectangular), with $<\delta y> = 0$ and $<\delta y^2> = u(y)^2$, where $u(y)$ is the standard uncertainty in $y$. In practice, we do this by choosing a random number from the standard normal distribution (i.e., mean of zero, variance of 1) and multiplying by the standard uncertainty. For complex quantities, the real and imaginary parts are simulated separately. In principle we could include correlation between errors in the real and imaginary parts or work with uncertainties in magnitude and phase, but we have not yet done so.

Because the input variables include sets of variables that are all measured in the same manner, correlated errors can and do occur, and the correlations can cause significant effects in the noise-parameter uncertainties [6,15]. We therefore include correlated errors in the simulations. The correlations that we include are among all the measured reflection coefficients and the S-parameters, among all the output noise temperatures, and among the temperatures of the ambient-temperature terminations. If there is more than one nonambient input termination, we include correlations between them. The way that correlated errors are simulated is to add an additional term to eq. (23). If $y_i$ and $y_j$ are two physical quantities whose errors are correlated (at least in part), we write

$$\begin{aligned} y_i(sim) &= y_{i,0} + \delta y_i(unc) + \delta y_i(cor), \\ y_j(sim) &= y_{j,0} + \delta y_j(unc) + \delta y_j(cor). \end{aligned} \tag{24}$$

The correlated (*cor*) and uncorrelated (*unc*) error terms satisfy $\langle \delta y_i(cor) \rangle = \langle \delta y_i(unc) \rangle = 0$, $\langle \delta y_i(cor)^2 + \delta y_i(unc)^2 \rangle = u_{cor}(y_i)^2 + u_{unc}(y_i)^2 = u(y_i)^2$, and similarly for $y_j$. The random errors for the uncorrelated error terms are chosen independently, whereas the same random number (scaled by the appropriate uncertainty in each case) is used for both correlated error terms. The correlation coefficient is given by

$$\begin{aligned} \rho_{ij} &= \frac{\left\langle \left(\delta y_i(unc) + \delta y_i(cor)\right)\left(\delta y_j(unc) + \delta y_j(cor)\right) \right\rangle}{u(y_i)u(y_j)} \\ &= \frac{\left\langle \delta y_i(cor)\delta y_j(cor) \right\rangle}{u(y_i)u(y_j)} = \frac{u_{cor}(y_i)u_{cor}(y_j)}{u(y_i)u(y_j)}. \end{aligned} \tag{25}$$

Each set of simulated noise-temp measurements is analyzed in the same manner as a set of real measurements: we perform a least-squares fit to the measurement results and obtain a set of the noise parameters ($X_1$, $X_2$, $X_{12}$, $G_0$). From these and the simulated measurement results for the amplifier's S-parameters, we compute the set of IEEE noise parameters ($T_{min}$, $t$, $\Gamma_{opt}$, $G_0$). This is done for each of the $N_{sim}$ sets of simulated measurements. The average and standard deviation of the measured values for each parameter ($X$ and IEEE) are computed. The (type-B) uncertainty in a single measurement of a parameter is then computed by combining the standard deviation in quadrature with the difference between the average and the true value. This is just the root-mean-square error (RMSE) of the sample,

$$u_B(y) = RMSE(y) = \sqrt{Var(y) + (\overline{y} - y_{true})^2} \ , \tag{26}$$

where $y$ is any of the noise parameters, and $Var(y)$ is the variance of the sample of simulated results for $y$. For the complex quantities $X_{12}$ and $\Gamma_{opt}$, statistics are done on the real and imaginary parts separately. The fact that $\overline{y}$ is not equal to the true value, may be unsettling at first, but such are the vagaries of nonlinear functions.

### 4.3 Input Uncertainties

The simulations require as input not just the true values of all parameters, but also the standard uncertainties in the parameters that are directly measured, i.e., the amplifier S-parameters, the reflection coefficients of all terminations, the noise temperatures of all terminations, the output reflection coefficient, $\Gamma_{2,i}$ in Fig. (2a), if it is measured, and the output noise temperatures. These input uncertainties (or the parameters that determine the uncertainties) are read into the Monte Carlo program along with the input data, so that they can be changed at any time, but we have a standard set of uncertainties that we usually use. This set is subject to change in the future, as we improve our knowledge of the uncertainties, and especially of the correlated errors.

The reflection coefficients $\Gamma_{G,i}$ and $\Gamma_{2,i}$ (if it is measured), are measured on a commercial vector network analyzer (VNA). Since all reflection coefficients are measured with the same calibration on the same VNA, there is significant correlation among the errors of the different reflection coefficients. The connector used on the radiometer port is type PC-7, and so we

assume the packaged amplifier also has PC-7 connectors. (If the amplifier has some other connector, requiring use of adapters, the uncertainty analysis is similar in form to the on-wafer case, which is treated in the next section.) The uncertainties in the reflection-coefficient measurements can depend on the magnitude of the reflection coefficient; usually the uncertainties are larger for larger reflection coefficients. Our program uses one value for small $|\Gamma|$ (less than or equal to 0.5) and another for large $|\Gamma|$ (greater than 0.5). In the program, we work in terms of $u_{cor}$ and $u_{unc}$, defined after eq. (24) above, and then compute $u$ and $\rho$ from them. The values typically used for small $|\Gamma|$ are $u_{cor} = 0.0025$ and $u_{unc} = 0.001$, corresponding to $u(\Gamma) \approx 0.002693$ and $\rho \approx 0.8621$. These uncertainties are somewhat larger than the manufacturer's specifications, reflecting our own past experience with such measurements [15]. For large $|\Gamma|$ we use $u_{cor} = 0.004$ and $u_{unc} = 0.001$, corresponding to $u(\Gamma) \approx 0.004123$ and $\rho \approx 0.9412$. The uncorrelated part of the uncertainty, $u_{unc} = 0.001$, is due primarily to connector (non)repeatability. The same $u(\Gamma)$ is used for both the real and the imaginary parts of each reflection coefficient, $u(\mathrm{Re}\Gamma) = u(\mathrm{Im}\Gamma) = u(\Gamma)$. The small S-parameters (i.e., $S_{11}$, $S_{22}$, and $S_{12}$) have their errors treated the same way as the reflection coefficients, including the correlations. For $S_{21}$ we use $u(\mathrm{Re}S_{21}) = u(\mathrm{Im}S_{21}) = 0.01$. This value was obtained by an extrapolation of the VNA specifications, which do not extend to $S_{21}$ magnitudes as large as we encounter. The input uncertainties in $S_{21}$ are not very important because the magnitude of $S_{21}$ is treated as a fitting parameter, $G_0 = |S_{21}|^2$.

The ambient temperature in the laboratory is set at 296.15 K and is kept within 0.5 K of this value. We therefore use a rectangular distribution extending from 295.65 K to 296.65 K for the ambient-temperature terminations. Because several hours intervene between measurements on the amplifier with different terminations, there is essentially no correlation between the errors in the temperatures of different ambient-temperature terminations.

In actual measurements of the output noise temperatures on NFRad [10], the measurement software evaluates and writes the uncertainty in the noise-temperature measurement. The uncertainty depends on a number of details, such as the reflection coefficient of the DUT, the magnitude of the noise temperature being measured, statistics of the multiple repeat measurements, and characteristics of the radiometer at the measurement frequency. Rather than perform a full evaluation of the uncertainty for each simulated measurement, we use the following approximate parameterization for the uncertainty in the noise-temperature measurements,

$$u(T_{meas}) = 0.2K + 0.005\left(T_{meas} - T_a\right), \tag{27}$$

where $T_a$ is the noise temperature corresponding to the ambient temperature of 296.15. This form is adequate provided that the reflection coefficient of the DUT is less than about 0.2. For larger reflection coefficients, further refinement is required, as described in Section 5.

There is significant correlation among the measurements of the output noise temperatures for the different terminations. An examination of the uncertainty analysis that was performed for noise-temperature measurements in coaxial lines [10,16] leads to the conclusion that most errors are correlated if all the reflection coefficients are measured with the same VNA calibration, as they typically are in the amplifier noise-parameter measurements. The major source of uncorrelated error is the connector (non)repeatability. The magnitude of the connector error

relative to the correlated errors would lead to a value $\rho \approx 0.98$. Because correlated errors in the noise-temperature measurements often lead to much smaller uncertainties [6], we are reluctant to use such a large correlation coefficient without being very sure of it. Until we have better knowledge of these correlations, we will use $\rho = 0.64$, which corresponds to $u_{cor}/u_{unc} = 4/3$. This may lead to a small overestimate of the uncertainty, but we prefer to err on the side of caution.

If two nonambient input terminations are used, there is a correlation between the errors in their noise temperatures if they are both measured on the same system, as is the case at NIST. We have investigated the case of one hot and one cold input noise source, and we find that if both are measured on NFRad, the correlation coefficient is $\rho \approx -0.115$. The negative sign occurs because the correlated errors have different sign for noise temperatures above and below ambient temperature. In principle, there is also a correlation between errors in measuring the output noise temperature from the amplifier and in measuring the nonambient input temperature(s), since both types of measurements are performed on the same radiometer (NFRad) with the same standards. In NIST measurements, this effect is usually small for the coaxial amplifier case because the nonambient input termination is usually measured with a different VNA calibration, often many months before the noise-parameter measurements. We have therefore ignored this correlation in the Monte Carlo program for the type-B uncertainties in the noise parameters for coaxial amplifiers. At many industrial laboratories, however, the same diode noise source that is used to calibrate the radiometer is also used as the hot input noise source. Furthermore, its noise temperature is one of the major sources of uncertainty. In this case, the correlation between errors in the hot input noise temperature and the measured output noise temperatures can be important.

### 4.4 Sample Results

We have recently measured the noise parameters of a low-noise amplifier (LNA) from 8 GHz to 12 GHz. This was done to test an automated variable-termination unit (VTU) [10], which can be used to automatically switch among a series of input terminations, greatly reducing the time required for the measurements. For these measurements, 11 different input terminations were used in the forward configuration, of which one was hot (between 1000 K and 1100 K, depending on frequency), one cold (about 100 K to 110 K) and the remainder at room temperature (about 296.15 K). In addition, one reverse measurement was done, with a matched load on the output of the LNA.

Results for the $X$ parameters are shown in Fig. 4. The quantity $X_2$ is the equivalent input noise temperature for a matched (reflectionless) input termination, often called the 50 Ω noise temperature. There are two sets of uncertainties plotted for $X_2$, to show the effect of an output attenuator on the measurements. The actual measurements were performed with a 20 dB attenuator on the amplifier's output (for the forward configuration), in order to keep the output noise temperature in the measurement range of NFRad. Consequently, the noise at the radiometer/DUT measurement plane is weighted 99 to 1 in favor of the attenuator over the amplifier, and the uncertainty suffers significantly. The larger uncertainties on $X_2$ in Fig. 4 correspond to the actual measurements, and the smaller uncertainties represent what could be achieved if no attenuator were needed.

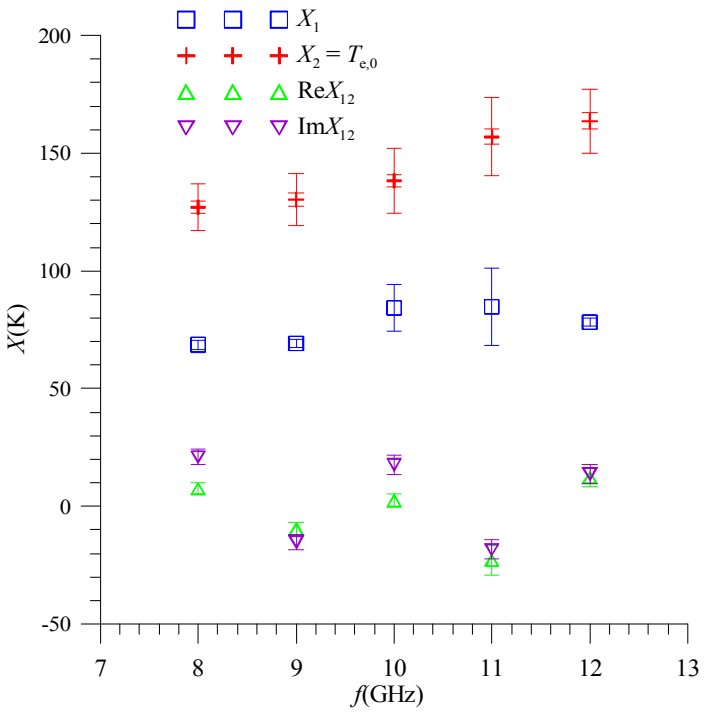


Figure 4. Results and uncertainties for $X$ parameters. The smaller set of uncertainties for $X_2$ applies to the case with no output attenuator in the measurements.

Another noteworthy point in Fig. 4 is the different sizes of the uncertainties for $X_1$ at different frequencies; they are much larger at 10 GHz and 11 GHz than at the other frequencies. A measurement of the reverse configuration gives the best determination of $X_1$, and one reverse measurement was made at each frequency. However, at some frequencies it is not possible to obtain a good least-squares fit when all the measured terminations are included. Presumably this is due to one (or occasionally two) bad measurements (which contribute disproportionately to $\chi^2$). In those cases, one (or two, if necessary) terminations are deleted, and at 10 GHz and 11 GHz it was necessary to exclude the reverse measurement, resulting in larger uncertainties for $X_1$.

In Fig. 5(a–f) we show the results for $G_0$ and the IEEE noise parameters. Because it is in common use, we have also shown the minimum noise figure in dB, which is related to $T_{min}$ by $F_{\min}(dB) = 10\log_{10}\left(1 + T_{\min}/T_0\right)$. As in Fig. 4, the two sets of uncertainties correspond to the actual measurements (larger uncertainties) and the case with no output attenuator (smaller uncertainties). For the phase of $\Gamma_{\text{opt}}$, Fig. 5(f), we show only the actual uncertainties, since they are so small. As for the $X$ parameters, the use of the attenuator causes a major increase in the uncertainties. The approximate values for the actual uncertainties are: 0.25 dB for $G_0$, 0.10 dB to 0.16 dB for $F_{min}$, 10 K to 17 K for $T_{min}$, 6 Ω to 12 Ω for $R_n$, 0.013 to 0.023 for $|\Gamma_{\text{opt}}|$, and 0.8° to 1.0° for $\phi_{opt}$. If an attenuator had not been necessary, these uncertainties would have been 0.05 dB for $G_0$, 0.03 dB for $F_{min}$, 2.5 K to 3.5 K for $T_{min}$, 0.08 Ω to 0.16 Ω for $R_n$, 0.003 to 0.007 for $|\Gamma_{\text{opt}}|$, and 0.2° to 0.5° for $\phi_{opt}$.

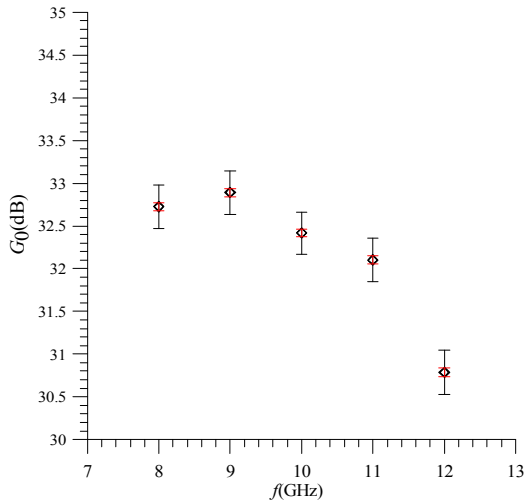


Fig. 5(a) Results and uncertainties for $G_0$.

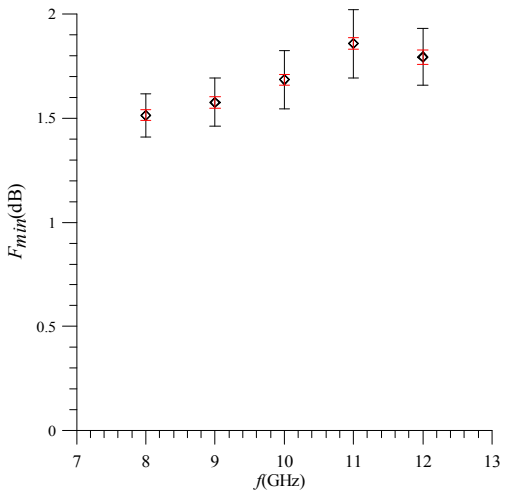


Fig. 5(b) Results and uncertainties for $F_{min}$.

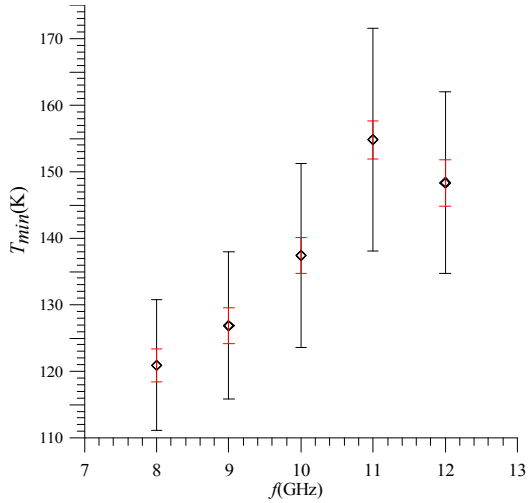


Fig. 5(c) Results and uncertainties for $T_{min}$.

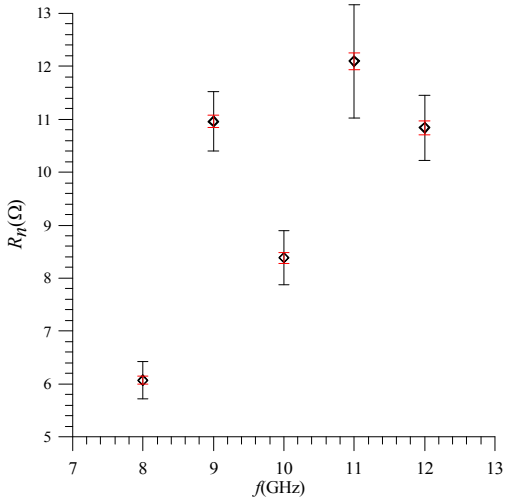


Fig. 5(d) Results and uncertainties for $R_n$.

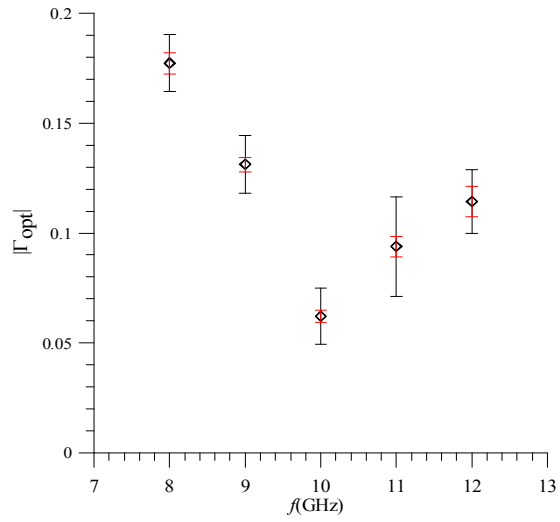


Fig. 5(e) Results and uncertainties for $|\Gamma_{opt}|$.

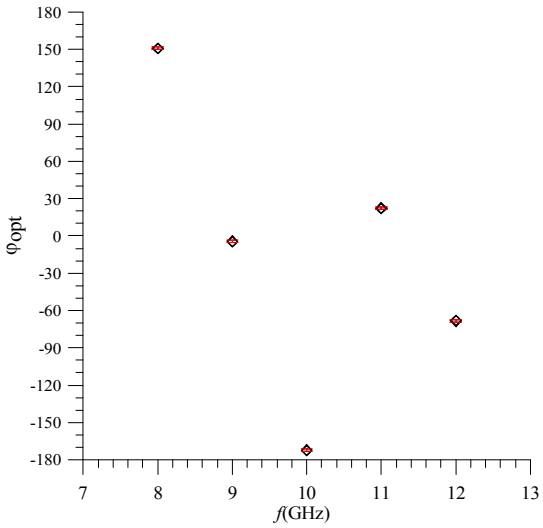


Fig. 5(f) Results and uncertainties for $\phi_{opt}$.

## 5. UNCERTAINTIES II: ON-WAFER MEASUREMENTS

### 5.1 Differences from the Coaxial Case

The measurement method for on-wafer noise-parameters is similar in principle to the method for measuring coaxial amplifiers, but additional complications arise because the measurement planes of interest are on-wafer, as indicated in Fig. 6. The reference planes for the DUT noise parameters are planes 1 and 2. The locations of the reference planes are chosen to assure single-mode conditions in the calibration process. An expanded view of the on-wafer structure for microstrip lines is shown in Fig. 7. We do not attempt to de-embed down to the transistor reference planes T1 and T2, as is often done in industry.

In order to use eqs. (6), (7), (18), and (19) between planes 1 and 2, we need the reflection coefficients, S-parameters, and noise temperatures at those planes. A two-tier calibration is performed using a multiline TRL set of calibration standards [17,18] that has been fabricated on the wafer. The NIST MultiCal® software is used to perform the two-tier calibration. The calibrated VNA is then used to measure the reflection coefficients and transistor S-parameters at planes 1 and 2, as in the amplifier case in the preceding section. The output noise temperatures are measured by NFRad at plane 2′ and corrected to plane 2, as described in Section 5.3 below. Similarly, the non-ambient input noise temperature is measured by NFRad using the configuration of Fig. 6, but with the on-wafer device replaced by a through line. Again, NFRad measures at plane 2′, and from that we compute the noise temperature at plane 1.

The uncertainty analysis for measurement of the noise parameters of on-wafer transistors is thus similar to that for measurements on packaged amplifiers, but it presents a few additional complications. Because the measurement planes of interest are on the wafer, we must characterize and correct for the effects of the probes, which introduces additional uncertainty. Also, the uncertainties in VNA and noise measurements are different on a wafer from what they are in coaxial lines, and therefore the input uncertainties are different for the on-wafer case. The third complication is that the transistor may be very poorly matched, leading to relatively large values of the reflection coefficient at its output. This requires that we refine our estimate of the uncertainty in measuring the output noise temperature. It also requires us to adopt a prescription for handling unphysical results in the simulations. We treat each of these complications in turn in the following subsections.

### 5.2 Input Uncertainties for On-Wafer Measurements

The uncertainty in the noise temperatures of the ambient-temperature terminations is the same as in the coaxial case above, and the uncertainties in the output noise temperatures and the nonambient input noise temperature are treated in the next subsection. Reflection coefficients and S-parameters measured at on-wafer reference planes have larger uncertainties than those measured at reference planes in coaxial lines. The input uncertainties that we use for the on-wafer reflection coefficients and S-parameters (other than $|S_{21}|$) are $u_{unc} = 0.004$ and $u_{cor} = 0.003$, corresponding to $u(\Gamma) = 0.005$ and $\rho = 0.36$. For on-wafer measurements, we (currently) use the same uncertainties for large and small $|\Gamma|$.

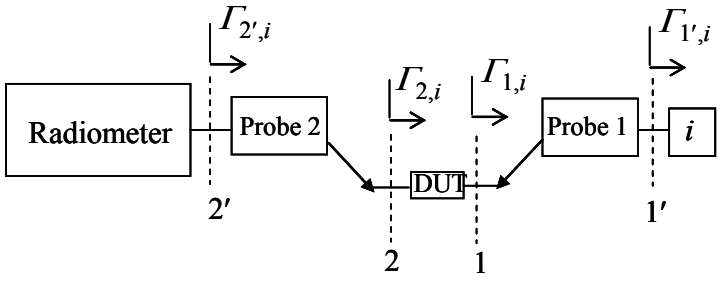


Figure 6. Reference planes for on-wafer measurements.

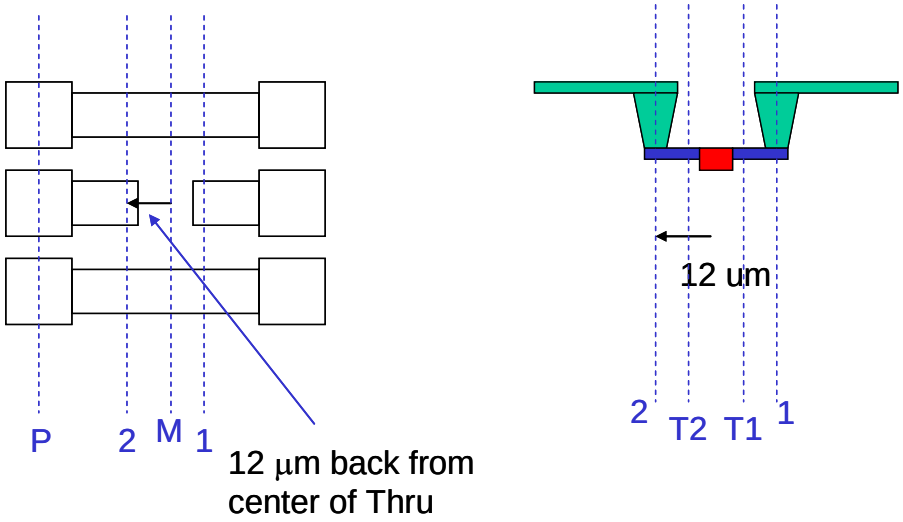


Figure 7. Detail of reference planes for transistor in microstrip.

### 5.3 Uncertainties in On-Wafer Noise Temperatures

The measurement planes of interest are on the wafer, as indicated in Fig. 6, whereas the noise-temperature measurements are performed by NFRad at plane 2′. We must therefore correct for the effect of Probe 2 to get the noise temperatures at plane 2. The S-parameters of the probe are determined in the two-tier calibration, as described in Section 5.1. To obtain the noise temperature at plane 2 $T_{2,i}$ from the noise temperature at plane 2′ $T_{2',i}$ , we treat the probe as an adapter, characterized by its available-power ratio $\alpha_{2'2,i}$ ,

$$\alpha_{2'2,i} = \frac{\left|S_{2'2}\right|^2\left(1-\left|\Gamma_{2,i}\right|^2\right)}{\left|1-\Gamma_{2,i}S_{22}\right|^2\left(1-\left|\Gamma_{2',i}\right|^2\right)}, \tag{28}$$

where $S_{2'2}$ is the S-parameter of probe 2 from plane 2′ to plane 2, $S_{22}$ is the reflection S-parameter of probe 2 at plane 2 (what would normally be called $S_{11}$), $\Gamma_{2,i}$ is the reflection coefficient at plane 2 (from the transistor), and $\Gamma_{2',i}$ is the reflection coefficient at plane 2′ (from the probe).

Knowing $\alpha_{2'2,i}$, we compute the output noise temperature at plane 2 in terms of $T_{2',i}$ in the usual manner,

$$T_{2,i} = \frac{T_{2',i} - (1 - \alpha_{2'2,i})T_a}{\alpha_{2'2,i}}, \tag{29}$$

where $T_a$ is the noise temperature of the probe, which is assumed to be at ambient temperature.

From eq. (29) we see that in order to compute the uncertainty in the on-wafer output noise temperature $T_{2,i}$, we need the uncertainties in $T_a$, $T_{2',i}$, and $\alpha_{2'2,i}$. The uncertainty in $T_a$ is the same as in the case of the coaxial amplifier measurements, treated above. The probe effect, of course, was absent from the treatment of the preceding section, and there is also a new complication with the noise measurement at the coaxial plane $T_{2',i}$. Because the on-wafer transistor may have a relatively large value of $|S_{22}|$, the reflection coefficient at the coaxial measurement plane $\Gamma_{2',i}$ can also be large. For values of $|\Gamma_{2',i}|$ larger than about 0.2, the uncertainty in $T_{2',i}$ increases, and the approximation of eq. (27) is no longer adequate. This occurs because as $|\Gamma_{2',i}|$ increases, the mismatch correction increases, and a larger mismatch correction magnifies any error in the measurement of the reflection coefficient. Examination of the radiometer equation for NFRad [11] reveals that $(T_{2',i} - T_a) \propto (1 - |\Gamma_{2',i}|^2)^{-1}$. Because eq. (28) indicates that $\alpha_{2'2,i} \propto (1 - |\Gamma_{2',i}|^2)^{-1}$ as well, we can effect some simplification by regrouping eq. (29),

$$\begin{aligned} T_{2,i} &= \frac{1}{\alpha}\left(T_{2',i} - T_a\right) + T_a \\ &= \frac{1}{\alpha'} T_{2',i}{}' + T_a , \end{aligned} \tag{30}$$

where we have suppressed the subscripts on $\alpha$ for convenience, and pulled out and cancelled factors of $(1 - |\Gamma_{2',i}|^2)$ by defining $\alpha' \equiv (1 - |\Gamma_{2',i}|^2)\alpha$ and $T_{2',i}' \equiv (1 - |\Gamma_{2',i}|^2) \times (T_{2',i} - T_a)$. The advantages of the form in eq. (30) are that it removes the necessity of dealing with important correlations between the errors in $\alpha$ and $T_{2',i}$, and that we can use eq. (27) for the uncertainty in $T_{2',i}'$. From the usual rules for propagation of uncertainty [5], the uncertainty in $T_{2,i}$ can be written as

$$u^2(T_{2,i}) = \frac{1}{\alpha'^2} u^2(T_{2',i}{}') + \frac{(T_{2,i} - T_a)^2}{\alpha'^2} u^2(\alpha') + u^2(T_a), \tag{31}$$

where we have used $T_{2',i}'/\alpha' = T_{2,i} - T_a$ in the second term on the right side.

As already mentioned, $u(T_{2',i}')$ and $u(T_a)$ can be treated as in the coaxial amplifier case above. For $\alpha'$ we use its definition and eq. (28), along with the propagation of uncertainty, to write

$$u^2(\alpha') \approx \left(\frac{2\alpha'}{|S_{2'2}|}\right)^2 u^2(|S_{2'2}|) + \left(\frac{2\alpha'|\Gamma_{2,i}|}{1-|\Gamma_{2,i}|^2}\right)^2 u^2(|\Gamma_{2,i}|), \tag{32}$$

where a small term has been discarded. The uncertainty for on-wafer reflection-coefficient measurements was discussed in the preceding subsection. The relevant numbers for use in eq. (32) are $u(|S_{2'2}|) = u(|\Gamma_{2,i}|) = 0.005$.

A final complication is that we sometimes need to use an attenuator at the output of probe 2 (plane 2′) in order to keep the measured noise temperature within the dynamic range of the radiometer NFRad. If an output attenuator is present, it can be lumped with the output probe, and the combined available power ratio is given by the product of the available power ratios of the attenuator and the probe, $\alpha_{total} = \alpha_{att}\alpha_{probe}$. In forming $\alpha'$, $\Gamma_{2',i}$ is to be taken at the attenuator output, between the attenuator and the radiometer. From eq. (31) we can see that using an attenuator degrades the uncertainty somewhat due to the smaller value for $\alpha'$. There is no effect on the second and third terms on the right hand side because $u^2(\alpha') \propto \alpha'^2$, but the first term increases somewhat.

Pulling everything together, we use eq. (31) for the uncertainty $u(T_{2,i})$ in noise-temperature measurements at the on-wafer reference plane 2. We get $u(T_{2',i}')$ from eq. (27) and $u(\alpha')$ from eq. (32). Equation (31) applies not only to the measured noise temperatures at the DUT output, but also to the measurement of the hot (or cold) input noise temperature. We have checked that the uncertainties obtained in this manner are consistent with the uncertainties that were confirmed in our earlier work [19,20] on verification and consistency checks for on-wafer noise-temperature measurements.

There is still the question of correlations among the errors in the measurements of the output noise temperatures $T_{2,i}$ and also between the errors in $T_{2,i}$ and those in the noise temperature of the hot or cold input termination. Of the three terms on the right side of eq. (31), the first term corresponds to the highly correlated errors in coaxial noise-temperature measurements ($\rho = 0.64$), considered in Section 4.3 above. The second term is comparable in size, but the errors contributing to it are mostly uncorrelated, because the sign and magnitude of $\alpha'$ vary randomly from one termination to another. The third term also corresponds to uncorrelated errors, but it is small relative to the other two terms. These considerations lead us to use $\rho_{ij} = 0.36$ for the correlation coefficient between errors in measurements of the on-wafer noise temperatures $T_{2,i}$ and $T_{2,j}$. As for the correlation between measurements of the output noise temperatures and of the on-wafer noise temperatures of the nonambient input terminations, we expect this correlation to be larger than in the coaxial case (Section 4.3) because the on-wafer measurements are performed with the same VNA calibration, on the same NFRad port, with not too long a time between. However, at present, we neglect this correlation, as we do in the coaxial case. We hope to include this effect in the future.

For perspective, it should be remembered that $u(T_{2,i})$ in eq. (31) is the uncertainty that is used for the simulated output noise-temperature measurement for a given termination $i$. Each output noise temperature in each set of simulated measurements has such an associated uncertainty, and these uncertainties are used to determine the weighting factors in the least-

squares fit in eq. (20). That fit then produces the simulated measured noise parameters for that set, and there are $N_{sim}$ such simulated measurement sets.

### 5.4 Occurrence and Treatment of Unphysical and Other "Bad" Results

The final additional complication with which we must deal in on-wafer simulations is the occurrence of unphysical results, those that violate the physical bounds discussed in Section 2.3. For the CMOS transistors that we have measured [4,21], it is quite possible to obtain unphysical results in the simulated measurements (as well as in real measurements). In a real measurement, we would normally discard such results and repeat the measurements. In the uncertainty program, we compute two sets of uncertainties, one with the unphysical results discarded, as we would usually do in practice, and one with the unphysical results included. One reason for evaluating the uncertainties with the unphysical results included is that if real measurements produce an unphysical result, we will probably want to evaluate the uncertainties in those results, in order to see whether they are consistent with physical results within the measurement uncertainties. To evaluate the uncertainties in unphysical real measurement results, we need to include the simulated unphysical results in the calculation.

We impose two further cuts on the set of simulated results. If the best fit is not good enough, we discard that set of simulated measurements, as we would with a set of real measurements that did not admit a good enough fit. For this purpose we define "good enough" by $\chi^2/\nu \leq 1$, where $\nu$ is the number of degrees of freedom in the fit. In several instances, we have also evaluated the uncertainties with a cut of $\chi^2/\nu \leq 1.5$, and it makes little difference. The other cut is on the uncertainty in $\Gamma_{opt}$. It sometimes happens that an acceptable fit is obtained, but that the variance of $\Gamma_{opt}$ is enormous (corresponding to an extremely flat minimum in this variable). A real measurement set with this property would be discarded, and we do so in the simulation as well. The maximum standard deviation allowed for either the real or imaginary part of $\Gamma_{opt}$ is 1.

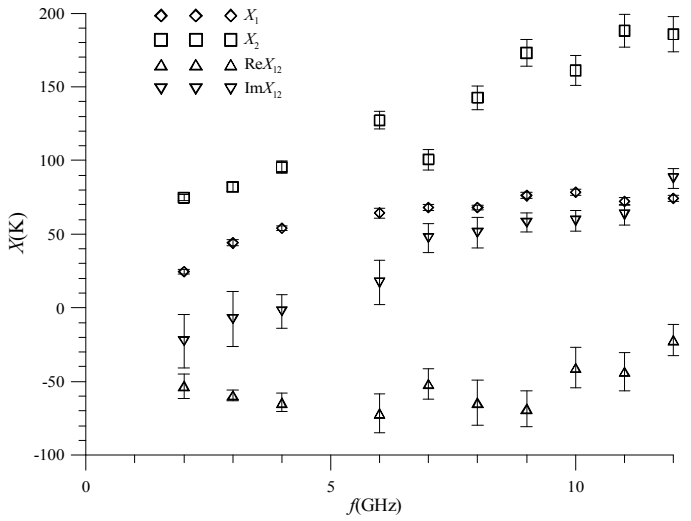


Figure 8. Results and uncertainties for $X$ parameters of a transistor on a wafer.

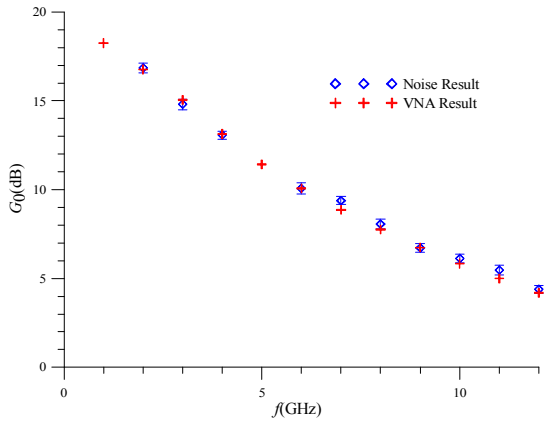


Fig. 9(a) Results and uncertainties for $G_0$.

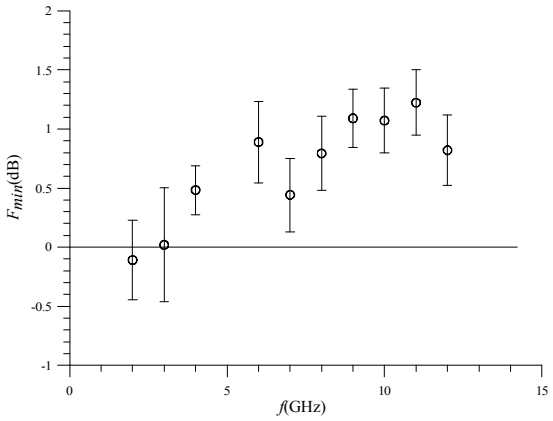


Fig. 9(b) Results and uncertainties for $F_{min}$(dB).

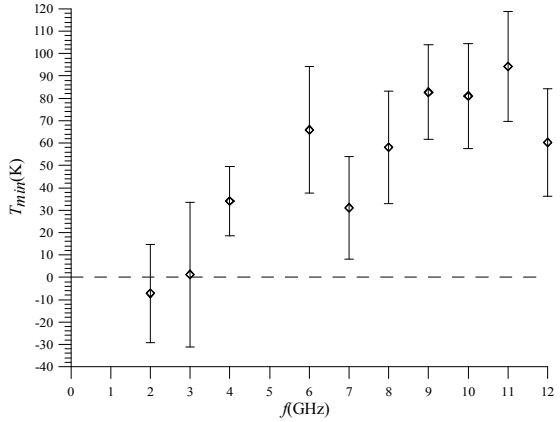


Fig. 9(c) Results and uncertainties for $T_{min}$.

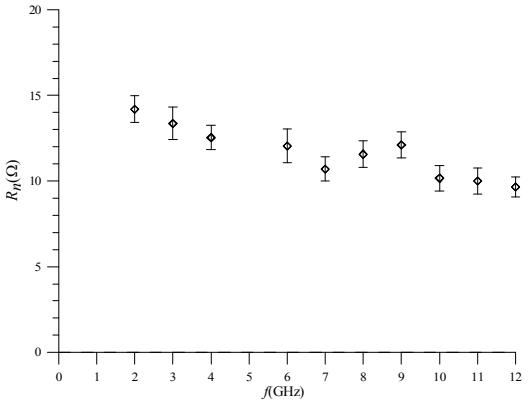


Fig. 9(d) Results and uncertainties for $R_n$.

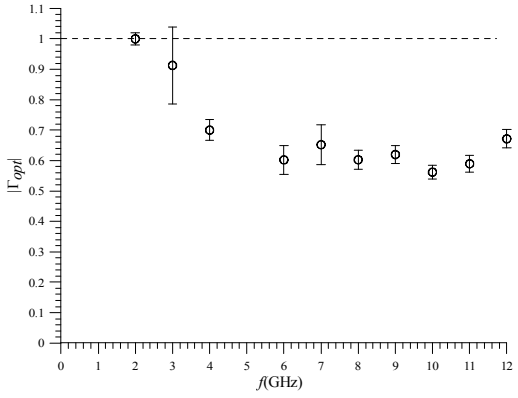


Fig. 9(e) Results and uncertainties for $|\Gamma_{opt}|$.

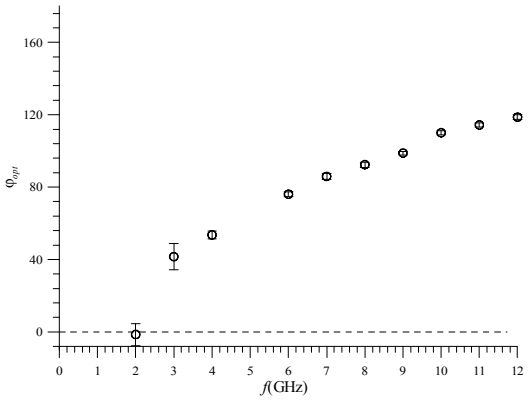


Fig. 9(f) Results and uncertainties for $\phi_{opt}$.

### 5.5 Sample Results

The preceding analysis was used for measurements of the noise parameters of an on-wafer transistor fabricated in 0.13 μm CMOS technology [4]. The set of input terminations for the forward configuration comprised one hot source (around 1100 K) and eight ambient-temperature terminations (296.15 K). One reverse measurement was also made, with a matched load connected at plane 1′. In the forward measurements, a 10 dB attenuator was connected between probe 2 and the radiometer, to keep the measured noise within the linear range of the radiometer. The results for the $X$ parameters are shown in Fig. 8 and those for $G_0$ and the IEEE noise parameters in Fig. 9 (a–f).

For $G_0$ we have shown a comparison to the value obtained from the VNA measurements. It is reassuring that the independent measurements generally agree within the uncertainties. The approximate values for the uncertainties in the on-wafer noise parameters are: 0.22 dB to 0.30 dB for $G_0$, 0.2 dB to 0.3 dB for $F_{min}$, 15 K to 25 K for $T_{min}$, 0.6 Ω to 0.8 Ω for $R_n$, 0.02 to 0.07 for $|\Gamma_{\rm opt}|$, and 1° to 6° for $\phi_{opt}$. As expected, the uncertainties in the on-wafer case are generally somewhat larger than for the connectorized amplifier. As in the amplifier case above, if the measurements could be done without an output attenuator, the uncertainties would be smaller.

## 6. SUMMARY

We have set forth the uncertainty analysis for NIST measurements of the noise parameters of amplifiers and transistors, where the reference planes can be either in coaxial transmission lines or on a wafer. The standard uncertainty is the root sum of the squares of the type A and type B uncertainties. The type A uncertainties are determined in the weighted least-squares fit to the overdetermined system of equations that result from the measurements of the output noise temperatures for different configurations and terminations. The type B uncertainties are evaluated by a Monte Carlo procedure. The program that is used to perform the Monte Carlo computation is described in Appendix B. The uncertainty analysis described has been used for both coaxial low-noise amplifiers [3] and very poorly matched on-wafer CMOS transistors [4,20]. In the amplifier case [3], the results were subjected to checks and verification that confirmed the general validity of the uncertainties, as well as the actual values of the parameters.

---

I am grateful to Dave Walker of NIST for many discussions and for performing the measurements to which this analysis is applicable. I also thank Ken Wong of Agilent for suggesting/requesting this paper. This work was supported in part by a contract from Agilent Corp.

## REFERENCES

[1] D. Wait and G. F. Engen, Application of radiometry to the accurate measurement of amplifier noise, IEEE Trans. Instrum. Meas. 40: 433–437 (1991).

[2] D. F. Wait and J. Randa, Amplifier noise measurement at NIST, IEEE Trans. Instrum. Meas. 46: 482–485 (1997).

[3] J. Randa and D. Walker, Amplifier noise-parameter measurement checks and verification, Digest, 63rd ARFTG Conf., pp. 41–45 (2004).

[4] J. Randa and D.K. Walker, On-wafer measurement of transistor noise parameters at NIST, IEEE Trans. Instrum. Meas. 56(2): 551–554 (April 2007).

[5] ISO Guide to the Expression of Uncertainty in Measurement, International Organization for Standardization; Geneva, Switzerland (1993).

[6] J. Randa, Noise-parameter uncertainties: A Monte Carlo simulation, J. Res. Natl. Inst. Stand. Technol. 107: 431–444 (2002).

[7] S. Wedge and D. Rutledge, Wave techniques for noise modeling and measurement, IEEE Trans. Microwave Theory Tech. 40: 2004–2012 (November 1992).

[8] J. Randa, T. McKay, S. L. Sweeney, D. K. Walker, L. Wagner, D. R. Greenberg, J. Tao, and G. A. Rezvani, Reverse noise measurement and use in device characterization, 2006 IEEE Radio Frequency Integrated Circuits (RFIC) Symposium Digest, pp. 345–348, San Francisco (June 2006).

[9] H. Haus et al., IRE standards on methods of measuring noise in linear twoports 1959, Proc. IRE, 48: 60–68 (1960).

[10] D. Gu, D. K. Walker, and J. Randa, Noise-parameter measurement with automated variable terminations, submitted to 2008 Conference on Precision Electromagnetic Measurements (CPEM 2008), Broomfield, CO (June 2008).

[11] C. A. Grosvenor, J. Randa, and R. L. Billinger, Design and testing of NFRad—A new noise measurement system, NIST Tech. Note 1518 (March 2000).

[12] D. Luenberger, Linear and Nonlinear Programming, Ch. 7.8, Second ed. Reading, MA: Addison-Wesley (1984).

[13] W. H. Press, B. P. Flannery, S. A. Teukolsky, and W. T. Vetterling, Numerical Recipes, Chap. 14.5, Cambridge: Cambridge University Press (1986).

[14] J. Randa and W. Wiatr, Monte Carlo estimation of noise-parameter uncertainties, IEE Proceedings—Science, Measurement and Technology, 149: 333–337 (2002).

[15] J. Randa, Simulations of noise-parameter uncertainties, 2002 IEEE MTT-S International Microwave Symposium Digest, Seattle, WA, pp. 1845–1848 (2002).

[16] J. Randa, Uncertainties in NIST noise-temperature measurements, NIST Tech. Note 1502 (March 1998).

[17] R. Marks, A multi-line method of network analyzer calibration, IEEE Trans. Microwave Theory Tech., 39(7): 1205–1215 (July 1991).

[18] D. Williams and R. Marks, Transmission line capacitance measurement, IEEE Microwave Guided Wave Lett., 1(9): 243–245 (September 1991).

[19] J. Randa, Noise temperature measurements on wafer, NIST Tech. Note 1390 (March 1997).

[20] J. Randa, R. L. Billinger, and J. L. Rice, On-wafer measurements of noise temperature, IEEE Trans. Instrum. Meas., 48(6): 1259–1269 (December 1999).

[21] J. Randa, S. L. Sweeney, T. McKay, D. K. Walker, D. R. Greenberg, J. Tao, J. Mendez, G. A. Rezvani, and J. J. Pekarik., Interlaboratory comparison of noise-parameter measurements on CMOS devices with 0.12 μm gate length, Digest, 66th ARFTG Conf., pp. 77-81 (2005).

## APPENDIX A: JACOBIAN MATRIX FOR $X \rightarrow$ IEEE

In order to compute the type-A uncertainties in the IEEE noise parameters from eq. (22), we need the elements of the Jacobian matrix for the transformation from $X$-parameters to the IEEE parameters. It is a straightforward exercise to compute them, and we present them here.

The easiest elements are the partial derivatives of $t = 4R_nT_0/Z_0$, which in terms of the $X$'s is given by

$$t = X_1 + \left|1 + S_{11}\right|^2 X_2 - 2\,\mathrm{Re}\left[\left(1 + S_{11}\right)^* X_{12}\right]. \tag{A.1}$$

The relevant partial derivatives are

$$\frac{\partial t}{\partial X_1} = 1, \quad \frac{\partial t}{\partial X_2} = \left|1 + S_{11}\right|^2, \quad \frac{\partial t}{\partial\, \mathrm{Re}\, X_{12}} = -2(1 + \mathrm{Re}\, S_{11}), \quad \frac{\partial t}{\partial\, \mathrm{Im}\, X_{12}} = -2\,\mathrm{Im}\, S_{11}. \tag{A.2}$$

We consider $\Gamma_{opt}$ next because it is used in writing $T_{min}$. The expression for $\Gamma_{opt}$ is

$$\begin{aligned} \Gamma_{opt} &= \frac{\eta}{2}\left(1 - \sqrt{1 - \frac{4}{|\eta|^2}}\right), \\ \eta &= \frac{X_2\left(1 + \left|S_{11}\right|^2\right) + X_1 - 2\,\mathrm{Re}\left(S_{11}^* X_{12}\right)}{\left(X_2 S_{11} - X_{12}\right)}. \end{aligned} \tag{A.3}$$

We treat the real and imaginary parts of $\Gamma_{opt}$ separately. The partial derivatives can all be written in terms of partial derivatives of $\eta$,

$$\begin{aligned} \frac{\partial\, \mathrm{Re}\, \Gamma_{opt}}{\partial X_i} &= \frac{1}{2}\left(1 - \sqrt{1 - \frac{4}{|\eta|^2}}\right)\frac{\partial\, \mathrm{Re}\, \eta}{\partial X_i} - \frac{\mathrm{Re}\, \eta}{|\eta|^4\sqrt{1 - \frac{4}{|\eta|^2}}}\frac{\partial |\eta|^2}{\partial X_i}, \\ \frac{\partial\, \mathrm{Im}\, \Gamma_{opt}}{\partial X_i} &= \frac{1}{2}\left(1 - \sqrt{1 - \frac{4}{|\eta|^2}}\right)\frac{\partial\, \mathrm{Im}\, \eta}{\partial X_i} - \frac{\mathrm{Im}\, \eta}{|\eta|^4\sqrt{1 - \frac{4}{|\eta|^2}}}\frac{\partial |\eta|^2}{\partial X_i}. \end{aligned} \tag{A.4}$$

The derivatives of $\eta$ are given by

$$\begin{aligned}
\frac{\partial \operatorname{Re}\eta}{\partial X_i} &= \operatorname{Re}\left(\frac{\partial \eta}{\partial X_i}\right),\ \frac{\partial \operatorname{Im}\eta}{\partial X_i} = \operatorname{Im}\left(\frac{\partial \eta}{\partial X_i}\right), \\
\frac{\partial |\eta|^2}{\partial X_i} &= 2\left(\operatorname{Re}\eta \frac{\partial \operatorname{Re}\eta}{\partial X_i} + \operatorname{Im}\eta \frac{\partial \operatorname{Im}\eta}{\partial X_i}\right),
\end{aligned} \tag{A.5}$$

where

$$\begin{aligned}
\frac{\partial \eta}{\partial X_1} &= \frac{1}{X_2 S_{11} - X_{12}}, \\
\frac{\partial \eta}{\partial X_2} &= \left(1 + |S_{11}|^2 - \eta S_{11}\right)\frac{\partial \eta}{\partial X_1}, \\
\frac{\partial \eta}{\partial \operatorname{Re} X_{12}} &= \frac{-2\operatorname{Re} S_{11} + \eta}{X_2 S_{11} - X_{12}}, \\
\frac{\partial \eta}{\partial \operatorname{Im} X_{12}} &= \frac{-2\operatorname{Im} S_{11} + j\eta}{X_2 S_{11} - X_{12}}.
\end{aligned} \tag{A.6}$$

Finally, we treat $T_{min}$, which is given by

$$T_{\min} = \frac{X_2 - \left|\Gamma_{opt}\right|^2\left[X_1 + |S_{11}|^2 X_2 - 2\operatorname{Re}\left(S_{11}^* X_{12}\right)\right]}{\left(1 + \left|\Gamma_{opt}\right|^2\right)}. \tag{A.7}$$

It is understood that in eq. (A.7), occurrences of $\Gamma_{opt}$ are just a shorthand way of writing the expression on the right side of eq. (A.3). The derivatives of $T_{min}$ are given by

$$\frac{\partial T_{\min}}{\partial X_1} = \frac{1}{1+\left|\Gamma_{opt}\right|^2}\left\{-\left|\Gamma_{opt}\right|^2 - \left[X_1 + \left|S_{11}\right|^2 X_2 - 2\,\mathrm{Re}\left(S_{11}^* X_{12}\right) + T_{\min}\right]\frac{\partial\left|\Gamma_{opt}\right|^2}{\partial X_1}\right\},$$

$$\frac{\partial T_{\min}}{\partial X_2} = \frac{1}{1+\left|\Gamma_{opt}\right|^2}\left\{\left(1-\left|\Gamma_{opt} S_{11}\right|^2\right) - \left[X_1 + \left|S_{11}\right|^2 X_2 - 2\,\mathrm{Re}\left(S_{11}^* X_{12}\right) + T_{\min}\right]\frac{\partial\left|\Gamma_{opt}\right|^2}{\partial X_2}\right\},$$

$$\frac{\partial T_{\min}}{\partial\,\mathrm{Re}\,X_{12}} = \frac{1}{1+\left|\Gamma_{opt}\right|^2}\left\{2\left|\Gamma_{opt}\right|^2\,\mathrm{Re}\,S_{11} - \left[X_1 + \left|S_{11}\right|^2 X_2 - 2\,\mathrm{Re}\left(S_{11}^* X_{12}\right) + T_{\min}\right]\frac{\partial\left|\Gamma_{opt}\right|^2}{\partial\,\mathrm{Re}\,X_{12}}\right\},$$

$$\frac{\partial T_{\min}}{\partial\,\mathrm{Im}\,X_{12}} = \frac{1}{1+\left|\Gamma_{opt}\right|^2}\left\{2\left|\Gamma_{opt}\right|^2\,\mathrm{Im}\,S_{11} - \left[X_1 + \left|S_{11}\right|^2 X_2 - 2\,\mathrm{Re}\left(S_{11}^* X_{12}\right) + T_{\min}\right]\frac{\partial\left|\Gamma_{opt}\right|^2}{\partial\,\mathrm{Im}\,X_{12}}\right\}, \tag{A.8}$$

where the derivatives of $|\Gamma_{opt}|^2$ are given by

$$\frac{\partial\left|\Gamma_{opt}\right|^2}{\partial X_i} = 2\,\mathrm{Re}\,\Gamma_{opt}\,\frac{\partial\,\mathrm{Re}\,\Gamma_{opt}}{\partial X_i} + 2\,\mathrm{Im}\,\Gamma_{opt}\,\frac{\partial\,\mathrm{Im}\,\Gamma_{opt}}{\partial X_i} \tag{A.9}$$

and eqs. (A.4) through (A.6).

## APPENDIX B: OVERVIEW OF THE FORTRAN PROGRAM

The type-B uncertainties in our noise-parameter measurements are evaluated with a Fortran Monte Carlo program called NIST_NP_UNC. In this appendix we give an overview of the structure of the program, discussing each subprogram in turn.

### B.1 MAIN

The main program first initializes a few parameters, including the number of simulations to be performed (NSET). It queries the user for the names of the output file (OUTFILE2), to which the final results are written, and the input file (INFILE), from which the input data are read. It also defines OUTFILE1, naming it TRASH.TXT, to which it will write the noise parameters from each of the simulated measurements sets. This file is usually discarded, but it enables one to examine some details of the individual measurement sets for diagnostic purposes, should the occasion arise. The character variable QUANT(9), where 9 indicates the dimension, contains the names of the nine quantities for which the program compiles statistics: $X_1$, $X_2$, Re$X_{12}$, Im$X_{12}$, $G_0$, $T_{min}$, $t$, Re$\Gamma_{opt}$, and Im$\Gamma_{opt}$.

After the initialization, MAIN reads the input data. The first line of data read from the input file consists of the values for NMEAS, CHAR1, AMB_DIST, CHI_CUT, ALPH0_AT, ALPH0_PR. NMEAS is the number of different measurements in each set, i.e., the number of different forward-configuration terminations plus the number of reverse-configuration measurements made in the actual measurement set from which the noise parameters were determined. CHAR1 is a character variable that is either 'Y' if the output reflection coefficients are measured directly, or 'N' if they are determined by cascading the input reflection coefficient with the amplifier or transistor S-parameters. AMB_DIST is a character variable that specifies the distribution for errors in the ambient temperature, either 'GAUS' for a normal distribution, or 'RECT' for a rectangular distribution. CHI_CUT is the maximum value of $\chi^2/\nu$ retained in the simulations, as discussed in Section 5.4. ALPH0_AT is the value of $|S_{21}|^2$ for the attenuator (if it is present; see Section 5.3). The other factors in the available power ratio $\alpha$ of the attenuator are computed during the course of the program. If no attenuator is present, a value of 1.0 is used. ALPH0_PR is the value of $|S_{21}|^2$ for the output probe, probe 2 in Fig. 6. The second line of the input file contains the "true" values for the noise parameters and $G_0$, whose variable names are X1, X2, X12R, X12I, G, where R and I refer to real and imaginary parts. The third line of the input file consists of amplifier or transistor S-parameters, in the order S11R, S11I, S12R, S12I, S21R, S21I, S22R, S22I. The program then reads the information for the individual measurements in each set, contained in lines 4 through 3+NMEAS of the input file, each line corresponding to one of the measurements. Each line contains values for the number of the measurement (1 through NMEAS), the configuration (1 for forward, 2 for reverse), the noise temperature of the input termination, the real and imaginary parts of the reflection coefficient of the input termination, and the real and imaginary parts of the output reflection coefficient (plane 2 in Fig. 2(a) or 6, or plane 1 in Fig. 2b). If the output reflection coefficients are not measured directly (CHAR1 = 'N'), then the last two entries are absent. After reading the termination information, the program computes the true values for the IEEE noise parameters and tests whether the true values of both the IEEE and the $X$ parameters satisfy the physical constraints. The final input quantities are the input uncertainties, which are read from the last five lines of the input file. The first of these final lines contains the correlated and uncorrelated uncertainties in

reflection coefficients, first for small reflection coefficients, then for large reflection coefficients (see Sections 4.2 and 5.3). The next line contains the correlated and uncorrelated uncertainties for $S_{21}$ and then the connector repeatability. We usually absorb the connector repeatability into the input uncertainties in the reflection coefficients, so that this entry is 0, but the option is there to enter it explicitly. The next line contains the correlated and uncorrelated uncertainties for noise temperatures near ambient, and the following (next to last) line has the uncertainties for the hot input termination, the cold input termination, and the correlation between the two (Section 4.3 or 5.3). The final line of the input file contains the correlated and uncorrelated uncertainties for the measurements of the output noise temperatures (Section 4.3 or 5.3).

Once all of the input file has been read, the program assigns the appropriate uncertainty to each of the quantities whose measurement will be simulated and initializes all the sums that will be computed in the Monte Carlo process. It then enters a loop, each pass through of which corresponds to one simulated measurement set. In the loop, the first step is to call the subroutine SET_MEAS, which generates a complete simulated set of measurements, and returns the results for S-parameters, reflection coefficients, input noise temperatures, and output noise temperatures. It next calls the subroutine FULL_FIT, which fits the simulated set of measurement results to get the noise parameters, in both the *X* and the IEEE representations. The results are added to the set of running sums that include both good and bad results. The program then checks the flags for "bad" results (Section 5.4), and, if the results are not bad, they are added to the running sums for good results. Thus, we have two sets of sums and averages, one for all results and one for only good results. After the Monte Carlo loop is completed, the rest of the main program just computes averages and standard deviations and writes the results to the output file. The input data are also written to the output file, to ensure that the results are associated with the correct input.

### B.2 Subroutine SET_MEAS

The subroutine SET_MEAS simulates a complete set of noise-parameter measurements. The true values and uncertainties of the variables to be measured are passed from the main program through a common block. The number of different output noise temperatures to be measured is NMEAS. The simulated measurement results are labeled by _M affixed to the variable, except in the case of the output noise temperatures, which are designated T_OUT. The uncertainty corresponding to each simulated T_OUT is also computed and passed back to MAIN, for use in the fit of the simulated results.

The subroutine begins by generating the value for the complex deviate G_DEV. This one complex value is used for the correlated parts of the errors in all the reflection coefficients and S-parameters (except $S_{21}$) in this set of measurements. The deviates are all generated by the function subprogram GAUSDEV, which returns a normally distributed deviate with zero mean and unit variance. The program then generates simulated measurements for the S-parameters and repeats the process for near-ambient noise temperatures and the reflection coefficients. Finally, there is a loop that generates a simulated value for each of the output noise temperatures, along with the associated uncertainty for each measurement. Each pass through the loop corresponds to one of the measurements. The measurement simulation is performed by calling the subroutine T_MEAS, and the associated uncertainty is then computed.

### B.3 Subroutine T_MEAS

This subroutine generates a single measurement of the output noise temperature from one of the ports of the DUT. The input information comprises the true values of the noise temperature and reflection coefficient of the source that is connected to the DUT, the true value of the reflection coefficient of the DUT-source combination, the configuration (forward or reverse), the true values or the S-parameters and noise parameters of the DUT, and the input correlated and uncorrelated uncertainties for the measured noise temperatures. These input uncertainties are not used directly as the standard deviations in the measured noise temperature, but are used to set the scale and correlation coefficient for the standard deviations (Section 4.2). The subroutine first computes the true value for the output noise temperature for the appropriate configuration (forward or reverse). It then computes the uncertainty that is to be associated with that measurement, taking into account the effects of potentially large reflection coefficients, the probe, and the output attenuator, if it is present (Section 5.3). A simulated measurement result is then generated. The present version of the program allows inclusion of an output attenuator either for all the measurements or for none at all. We plan to change this soon, to allow use of an attenuator on some, but not all the measurements of the output noise temperature.

### B.4 Subroutine FULL_FIT

This subroutine performs a weighted least-squares fit to minimize the function $\chi^2$ defined by eq. (20), thereby determining the noise parameters and $G_0$ of the DUT. This same subroutine is used in other applications as well, and consequently it includes some features that are not needed in this program. After some initial definitions, it calls the subroutine FWD_FIT, which performs a linear fit to all the forward measurements in the set. The results of this linear fit are used to generate an initial guess for use in the full nonlinear fit. The nonlinear fit also allows computation of the covariance matrix, which is used in other applications of FULL_FIT, but not here. If there are no reverse measurements included in the measurement set, the linear fit produces the full, correct results. Nevertheless, we perform the nonlinear fit in all cases in this subroutine because the covariance matrix is needed in the other applications, and the packaged program used for the linear fit does not allow computation of the covariance matrix. An odd feature of FULL_FIT is that we do not use the exact results of the linear fit as the initial guess for the nonlinear fit, but rather we multiply the linear-fit results by 0.9. The reason for this is that if the starting point for the nonlinear fitting program corresponds to the minimum of the function being minimized (as would be the case when the measurement set includes no reverse measurement), the program does not return the correct covariance matrix. (We have, of course, checked that the results of the nonlinear fit are independent of the initial guess and that it gives the same results as the linear fit when there are only forward measurements present.)

After the nonlinear fit, the subroutine checks that $\chi^2/\nu \leq$ CHI_CUT, computes the IEEE noise parameters from the $X$ parameters, and checks that the results satisfy the physical constraints. It then computes the Jacobian matrix for the transformation from $X$ parameters to IEEE parameters, which in this application is used only to check that the type-A uncertainty in $\Gamma_{opt}$ is not too large (Section 5.4).

### B.5 Subroutine FWD_FIT

The subroutine FWD_FIT performs a linear, weighted, least-squares fit to the output noise temperatures of a series of forward measurements. The relevant S-parameters, reflection coefficients, input noise temperatures, measured output noise temperatures, and uncertainties in the measured output noise temperatures are all passed to the program via a common block. The $X$ parameters and $G_0$ are determined by minimizing the $\chi^2$ defined in eq. (20). The minimization is performed by a packaged program that does a weighted, linear, least-squares fit.

### B.6 Subroutine FCN

This subroutine defines the "error" in a given measurement for purposes of the fit, i.e., it computes the difference between the measured value of the output noise temperature and the value computed from eq. (6) or (7) for the set of noise parameters $X$ and $G_0$. It is used in the nonlinear fitting routine, which minimizes the weighted sum of the squares of the errors for all the measurements in the set, as given by eq. (20).

### B.7 Subroutines GAUSDEV and RECTDEV

These two subroutines are taken from and explained in Chapter 7 of Reference [13]. RECTDEV returns a random deviate between 0.0 and 1.0, using a system-supplied random-number generator. The point of RECTDEV is that it eliminates correlations in k-space, which may be present in the system's random-number generator [13]. GAUSDEV generates and returns a normally distributed deviate with zero mean and unit variance, using RECTDEV as the source of uniform deviates.